Review of the influence of copper and chromium substitution on crystal structure, magnetic properties and magnetocaloric effect of GdFe2(Cu, Cr) (x = 0, 0.1, 0.15 and 0.2) intermetallic compounds

M. Saidi, Lotfi Bessais, M. Jemmali

J. Phys. Chem. Solids, 2022
Published article

Review of the influence of copper and chromium substitution on crystal structure, magnetic properties and magnetocaloric effect of $GdFe_{2-x}(Cu, Cr)_x$ (x = 0, 0.1, 0.15 and 0.2) intermetallic compounds

M. Saidi[1,2], L. Bessais[1*] and M. Jemmali[1,3]

Abstract

The iron-based compounds $GdFe_{2-x}(Cu,Cr)_x$ (x = 0, 0.1, 0.15 and 0.2) were synthesized successfully by means of arc-melting and annealing at 800°C for one week. The structural, magnetic and magnetocaloric properties of these intermetallic compounds were investigated systematically in detail using X-ray powder diffraction (XRD) analysis, Scanning electron microscopy (SEM) equipped with Energy dispersive X-ray spectroscopy (EDS), and magnetic measurements. The Rietveld analysis of X-ray diffraction patterns proves that $GdFe_{2-x}(Cu,Cr)_x$ (x = 0, 0.1, 0.15 and 0.2) compounds crystallize in the cubic laves phase $MgCu_2$-type structure with the $Fd\bar{3}m$ space group. Gadolinium and iron atoms statistically occupy the $8a$ and $16d$ sites respectively. Moreover, copper and chromium atoms substitute the iron atoms at site $8a$ in the $MgCu_2$-type structure. The temperature dependence of magnetization studied in a broad temperature range reveals that all compounds exhibit a ferromagnetic-paramagnetic transition at Curie temperature (T_C). We find that the substitution of iron by copper and chromium leads to a decrease in the magnetic ordering transition temperature. The Arrott plots of all our samples show the occurrence of a second-order phase transition. Besides, the performance of magnetocaloric effect (MCE) for $GdFe_{2-x}(Cu,Cr)_x$ (x = 0, 0.1, 0.15 and 0.2) compounds was evaluated by the magnetic entropy change (ΔS_M) and the related Relative Cooling Power (RCP). In the vicinity of T_C, the ΔS_M reached a maximum value of 0.79 J/kg.K, 1.2 J/kg.K, 1.4 J/kg.K and 2.5 J/kg.K, while the RCP was found to be 13.2 J/kg, 21.6 J/kg, 31.7 J/kg and 44.3 J/kg, respectively for $GdFe_{2-x}Cu_x$ (x = 0, 0.1, 0.15 and 0.2) compounds. Furthermore, the $GdFe_{2-x}Cr_x$ (x = 0.1, 0.15 and 2) compounds show ΔS_M values of about 0.9 J/kg.K, 1.3 J/kg.K and 1.8 J/kg.K, and RCP values of 14.8 J/kg, 25.4 J/kg and 36.8 J/kg respectively, under a field change of 1.56 T. Through these results, the $GdFe_{2-x}(Cu,Cr)_x$ (x = 0, 0.1, 0.15 and 0.2) compounds can be an attractive materials for use in magnetic refrigeration and heat pumping technology above room temperature.

Keywords

Intermetallic compounds; Magnetic materials; Magnetocaloric Effect.

[1] *University of Sfax, Faculty of Science, LSME, BP1171-3018 Sfax, Tunisia*
[2] *Univ. Paris Est Creteil, CNRS, ICMPE, 2 rue Henri Dunant F-94320 Thiais, France*
[3] *Department of Chemistry, College of Science and Arts, Ar-rass, Qassim University, PO Box 53, Buraydah Postcode 51921, Saudi Arabia*
[*] *Corresponding author, bessais@icmpe.cnrs.fr (L. Bessais).*

1. Introduction

Over recent years, human consciousness about energy and environment has been highly emphasized. The toxic gases associated with global-warming, greenhouse effects and ozone-depleting gases, such as chlorofluorocarbons (CFCs), hydrofluoric carbons (HFCs) and ammonia (NH_3) [1, 2] have posed a threat to human life, which limits the conventional gas-compression (CGC) refrigerators. Thus, from an environmental conservation perspective, research on future refrigeration technologies is increasingly oriented toward other techniques, such as magnetic refrigeration (MR), based on the magnetocaloric effect (MCE) [3, 4]. The principle of this effect is based on the reversible heating and cooling of a magnetic material after the application of a magnetic field variation [5, 6]. In addition, magnetic refrigeration is becoming a promising technology to replace the conventional cooling technique, because it is much more compactly built due to the fact of taking solid substances as working materials. The key advantage of magnetic refrigeration is that it has ecological, economic and environmental benefits [7, 8, 9, 10]. What is more, this technology doesn't cause atmospheric pollution or noise and it offers significantly more reliability and energy-efficient than the conventional refrigeration [11].

In this context, the intermetallic materials combining rare-earth elements and transition metals with large magnetocaloric

properties have attracted a considered attention owing to its potential application in the magnetic refrigeration (MR) technology [12, 13, 14, 15, 16, 17, 18, 19, 20, 21, 22, 23, 24].

Most of rare-earth transition-metals intermetallic compounds exhibit a second order magnetic transition (SOMT) [14, 16, 19, 20, 11]. Intermetallics that possess a SOMT generally exhibit negligible loss by thermal and magnetic hysteresis, consequently they could be a potential candidate for magnetic refrigeration.

In addition, many promising materials such as $Gd_5Si_2Ge_2$ [25, 26] $Mn_5Ge_{3-x}Si_x$ [27], and MnNiGa [28], have been broadly studied for their high magnetocaloric effect and their application as magnetic refrigerants.

Among numerous rare earth - transition metals-based intermetallic compounds, Laves-phases RM_2 (R stands for rare earth elements, and M stands for transition metals) compounds have been massively studied [29, 30]. These phases crystallize in three structure types: $MgCu_2$ (C15) type structure, $MgZn_2$ (C14) type structure, and $MgNi_2$ type structure (C36) [31]. The RV_2 (R = Ti, Nb, Hf, and Ta) compounds present high melting point, good oxidation resistance, and high strength at elevated temperatures which make them available for high-temperature structural applications [32, 33, 34] and hydrogen-storage [35]. In addition, the rare earth Laves phases RCo_2 (R= Dy, Ho, Er) [36, 37, 38, 39], $TbCo_2$ [40], $GdCo_2$ [41], and $SmNi_2$ [42] with cubic $MgCu_2$-type structure (C15) exhibit attractive and useful properties such as significant anisotropic magnetostriction, large magnetovolume effect, and large magnetocaloric effect around the Curie temperature.

In the literature, $GdFe_2$ compound, which crystallizes in the cubic Laves-phase with $MgCu_2$ type structure, has been the subject of many investigations in the past few years [43, 44, 45]. These compounds are of considerable scientific and technological interests because of their excellent magnetic, electronic, elastic and thermal properties, due to the coexistence of complementary features of itinerant ($3d$) and localized ($4f$) electrons in these compounds.

In our previous papers [46, 47], we have prepared a series of Gd-Fe-Cu and Gd-Fe-Cr alloys to determine the solid state phase equilibria in both ternary Gd-Fe-Cu and Gd-Fe-Cr systems at 800°C, through the use of SEM-EDS and XRD techniques. The solid solutions $GdFe_{2-x}Cu_x$ and $GdFe_{2-x}Cr_x$ were identified to exist in these isothermal sections, respectively, which extended from about $x = 0$ to $x = 0.2$. This outcome opens the way in this experimental work, for investigating the effect of copper and chromium substitution for iron on the structural, magnetic, and magnetocaloric properties of the $GdFe_{2-x}(Cu,Cr)_x$ (x = 0, 0.1, 0.15 and 0.2 compounds.

2. Experimental section

2.1 Synthesis

Samples with the total mass of 0.5 g were prepared from gadolinium (99.99 wt.%), iron (99.99 wt.%), copper (99.99 wt.%) and chromium (99.99 wt.%) metals. Prior to the melting process, calculated amounts of the elements were precisely weighed on a microbalance. Then, alloys were produced by melting the constituents in stoichiometric quantities in an electric arc furnace, in water-cooled copper mold with the use of a non-consumable tungsten electrode under protective argon gas. A piece of zirconium was used to remove traces of oxygen. Each sample was re-melted and turned over four to five times to achieve complete fusion and to obtain homogeneous state. After the melting procedure, the final mass of each buttons was checked. The weight loss did not exceed 1% of the initial total mass [46, 24]. After the melting procedure, the final mass of each buttons was checked. The weight loss did not exceed 1% of the initial total mass. After that, the melted samples were wrapped in Tantalum foil, vacuum-sealed in a quartz tube, and then annealed at 800°C for seven days to ameliorate the atomic diffusion kinetics. The annealing process was ended by quenching the samples in cold water in order to preserve their high temperature state. Thereafter, each prepared ingot was milled by means of an agate mortar to prepare powders for the different measurements.

2.2 Characterizations and measurements

The microstructural examination and metallographic investigation of the samples were made by means of a Merlin Scanning electron microscopy (SEM) with a Silicon Drift Detector (SDD)-X-Max. Quantitative energy dispersive X-ray spectroscopy (EDS) analysis was studied for quantitative phase analyses and composition measurement. Eventually, this characterization technique was performed to investigate the chemical composition and the morphological properties of the samples.

The crystallographic examination was performed by X-ray diffraction (XRD) patterns, recorded on a Bruker D8 diffractometer, using copper CuKα radiation (λ = 1.540562 Å). At room temperature, the data were registered over a 2θ ranging from 20° to 80°, with a step width of 0.015° and counting rate of 13.5 s. The X-ray patterns of $GdFe_{2-x}(Cu,Cr)_x$ (x = 0, 0.1, 0.15 and 0.2) compounds was refined by the Rietveld method [48, 49] using FULLPROF program [50, 51, 52, 53, 54, 55] so as to identify the present phase and to determine the lattice parameters.

Magnetic properties were measured as a function of temperature and magnetic field using a DSM-8 MANICS differential magnetometer [53, 54]. The temperature (T) dependence of magnetization (M) for $GdFe_{2-x}(Cu,Cr)_x$ (x = 0, 0.1, 0.15 and 0.2) compounds was determined from 300 K to 800 K and in applied magnetic field of 0.12 T. The Curie temperature (T_C) for each sample was determined as the minima in the dM/dT plots [56]. The magnetocaloric parameters were evaluated using the magnetic measurements data.

3. Results and discussion

3.1 Structure analysis

The Laves-phases represent the largest group of intermetallic compounds. More than 1400 binary and ternary Laves-phases

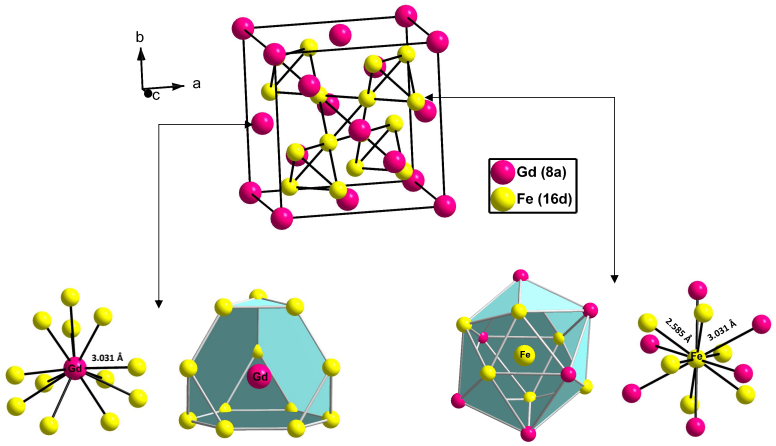

Figure 1. Crystal structure of $GdFe_2$ and coordination polyhedra for each crystallographic site.

were introduced in Pearsons Handbook of Crystallographic Data for Intermetallic Phases[57]. Laves-phases show a lot of interesting and useful properties such as excellent magnetic and magnetocaloric effects, corrosion and creep resistance properties. As a result, this class of intermetallics is strongly suggested for use as magneto-optical materials, hydrogen storage materials, magnetic and magnetocaloric materials [58, 59, 60]. These intermetallic phases are also named Friauf-Laves phases by Friauf who first studied the crystallographic their structures [61]. The stability of the AB_2 Laves-phase is ruled by the size ratio of atoms r_A/r_B equals: (3/2)1/2 = 1.225, where r_A and r_B are the average atomic radius of atoms occupying the A and B sites of the AB_2 crystal structure. These phases crystallize in three different kind of structure under the different conditions: the hexagonal type structure $MgZn_2$ (C14) and the double-hexagonal type structure $MgNi_2$ (C36) at high temperature, and the face centered cubic type structure $MgCu_2$ (C15) at low temperature [33].

The binary intermetallic compound $GdFe_2$ adopts the space group $Fd\bar{3}m$ with the point symmetry O_h^7 and the Pearson symbol cF24. This intermetallic compound belongs to the structure of the cubic Laves-phase $MgCu_2$ (C15) type. The gadolinium atoms have a face-centered structure and are structured relative to one another. However, the iron atoms are located in the corners of tetrahedral in the structure. This unit cell is formed by eight octants: gadolinium atoms occupy four octants, and the four iron tetrahedrons are located in the other four octants. The rare earth atoms Gd occupy the 8a Wyckoff site $(\frac{1}{8}, \frac{1}{8}, \frac{1}{8})$, and the transition metal atoms Fe are situated on the 16d site $(\frac{1}{2}, \frac{1}{2}, \frac{1}{2})$. The gadolinium atom is located at the center of a polyhedron named truncated tetrahedron formed by twelve iron atoms located in the corners. Besides, the iron atom at site 16d is surrounded by six iron atoms and six gadolinium ones. The lengths of $Fe-Fe$ bonds are equal to 2,585 (2) Å, whereas that of $Fe-Gd$ bonds are equal to 3.031 (4) Å as displayed in Figure 1. The detailed crystal structure of $GdFe_2$ compound and the coordination polyhedra for each Wyckoff site are shown in Figure 1. Iron and gadolinium atoms are drawn as yellow and pink circles, respectively.

The Rietveld refinement results of the X-ray diffraction patterns illustrate that the synthesized samples $GdFe_{2-x}(Cu,Cr)_x$ (x = 0, 0.1, 0.15 and 0.2) crystallize in the cubic $MgCu_2$ type structure ($Fd\bar{3}m$ space group). We show in Figure 2 the observed and calculated patterns as well as the difference profile of the $GdFe_2$, $GdFe_{1.8}Cu_{0.2}$ and $GdFe_{1.8}Cr_{0.2}$ compounds as an example. The set of bars corresponds to the calculated positions of the Bragg peaks of the refined compounds. It is clear from Figure 2 that all compounds exhibit a perfect pure cubic single Laves-phase nature. The high quality of the refinement is corroborated by the low value of the fit indicator χ^2 and R_B. It is noteworthy that the refinement analysis results show that copper and chromium substitute partially iron on Wyckoff site 16d. During this substitution of Fe by Cu and Cr in the $GdFe_{2-x}(Cu,Cr)_x$ (x = 0, 0.1, 0.15 and 0.2), the same $MgCu_2$-type structure was preserved. Table 1 summarizes the values of the crystallographic unit cell parameters, the reliability factors obtained from the best refinement, as well as the Gd, Fe, Cu and Cr occupation ratios.

The SEM-EDS analysis, which is in line with the results of the X-ray diffraction patterns, shows that all the prepared samples are single-phase. Figure 3 presents the SEM image micrograph of the $GdFe_{1.8}Cu_{0.2}$ compound (as an example). The grey area shows that this sample consists only of the $MgCu_2$-type structure without any impurity phase. The details of the measured compositions by EDS are listed as follows in Table 2.

In Figure 4, we plotted the variation of the cubic unit cell parameter (a) versus copper and chromium content x in the $GdFe_{2-x}Cu_x$ (x = 0, 0.1, 0.15 and 0.2) and $GdFe_{2-x}Cr_x$ (x = 0, 0.1, 0.15 and 0.2) compounds, respectively, obtained from the X-ray diffraction patterns refinement. The lattice parameter (a) of the $GdFe_2$ binary compound is equal to 7.430 Å. This value is in agreement with the value of 7.396 Å, previously reported by Buschow [62]. This slight difference of the lattice parameter could be due to the effect of the annealing step, or to the purity of the starting materials.

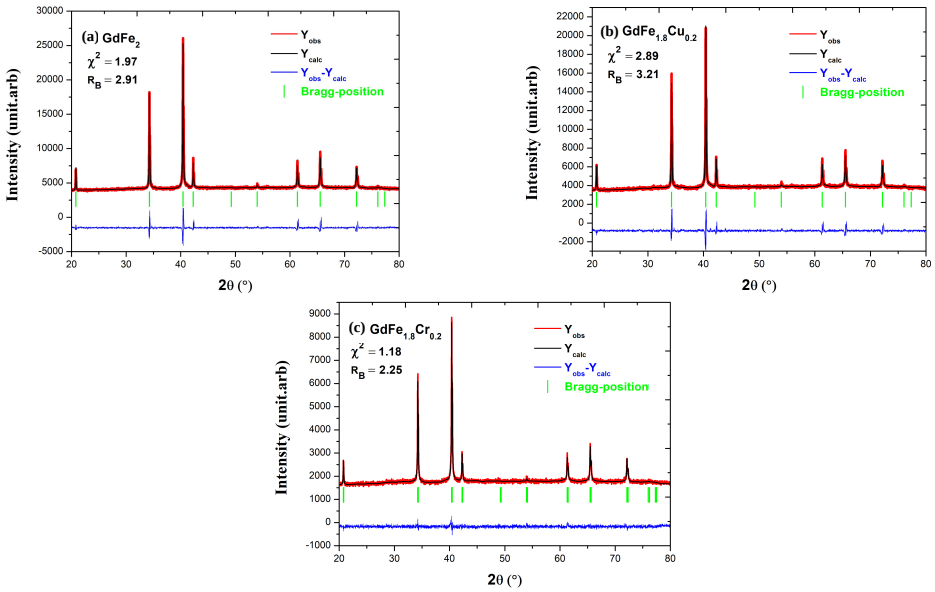

Figure 2. The Rietveld refinement of the X-ray powder diffraction patterns of $GdFe_2$, $GdFe_{1.8}Cu_{0.2}$ and $GdFe_{1.8}Cr_{0.2}$ compounds measured at room-temperature.

Table 1. XRD analysis results obtained by Rietveld method on the $GdFe_{2-x}(Cu, Cr)_x$ (x = 0, 0.1, 0.15 and 0.2) compounds.

Compounds	a (Å)	V (Å^3)	χ^2	R_B	Occupancy			
					Gd(8a)	Fe(16d)	Cu(16d)	Cr(16d)
$GdFe_2$	7.430(2)	410.172(4)	1.97	2.91	1	1	-	-
$GdFe_{1.9}Cu_{0.1}$	7.397(5)	404.731(3)	1.57	2.62	1	0.950	0.050	-
$GdFe_{1.85}Cu_{0.15}$	7.388(3)	403.255(8)	3.86	4.64	1	0.925	0. 075	-
$GdFe_{1.8}Cu_{0.2}$	7.382(8)	402.274(1)	2.89	3.21	1	0.90	0.10	-
$GdFe_{1.9}Cr_{0.1}$	7.439(3)	411.664(7)	2.96	3.98	1	0.95	-	0.50
$GdFe_{1.85}Cr_{0.15}$	7.453(5)	413.993(3)	1.64	1.18	1	0.925	-	0.075
$GdFe_{1.8}Cr_{0.2}$	7.460(2)	415.160(9)	1.18	2.25	1	0.90	-	0.10

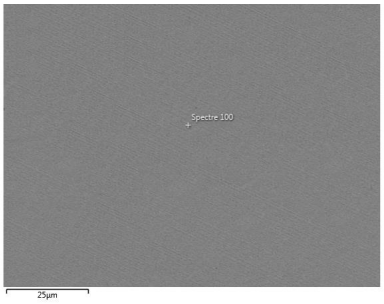

Figure 3. Backscattered electron SEM image of the $GdFe_{1.8}Cu_{0.2}$ compound.

Table 2. EDS results of the $GdFe_{2-x}(Cu, Cr)_x$ (x = 0, 0.1, 0.15 and 0.2) compounds.

Compounds	EDS results (at.%)			
	Gd	Fe	Cu	Cr
$GdFe_2$	33.4	66.6	-	-
$GdFe_{1.9}Cu_{0.1}$	33.3	63.35	3.35	-
$GdFe_{1.85}Cu_{0.15}$	33.3	61.66	5.04	-
$GdFe_{1.8}Cu_{0.2}$	33.4	60.02	6.58	-
$GdFe_{1.9}Cr_{0.1}$	33.2	63.40	-	3.40
$GdFe_{1.85}Cr_{0.15}$	33.2	61.68	-	5.12
$GdFe_{1.8}Cr_{0.2}$	33.2	60.04	-	6.66

From Figure 4, it can be seen that the lattice parameter (a) drop linearly with the increasing concentration of copper up to $x = 0.2$. This decrease is due to the smaller atomic radius size of copper (r = 1.45 Å) as compared to that of iron (r = 1.56 Å). On the contrary, a marked enhancement in the lattice parameter (a) was observed when increasing the chromium concentration (Figure 4). This expansion is due to the substitution of larger Cr atoms (r = 1.66 Å) for smaller Fe atoms.

Let's notice that, I.A. Al-Omari *et al.* [43] showed that the lattice parameter (a) of $GdFe_{2-x}Ti_x$ (x = 0, 0.05, 0.10, 0.15, 0.20, and 0.30) compounds raise with the increase of Titanium content, since the radius of Ti atom is larger than that of Fe. Furthermore, for the $YFe_{2-x}Al_x$ (x=0.3, 0.5, 0.7) compounds, Z. Li *et al.* [63] reported that substituting aluminium for iron

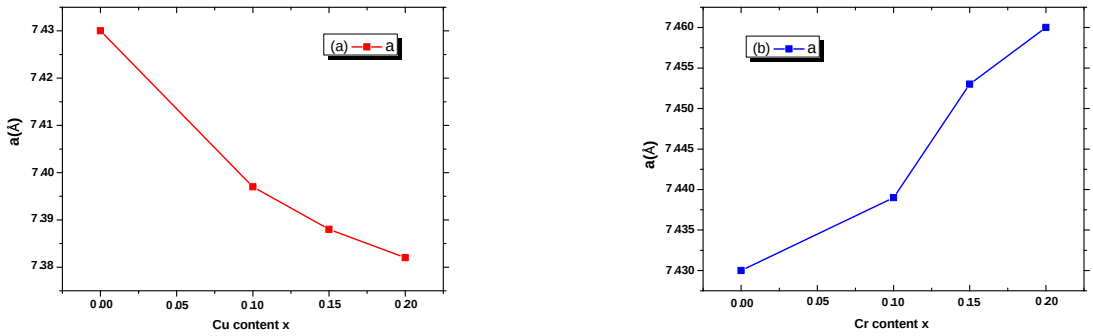

Figure 4. Variation of the lattice parameter a of (a) $GdFe_{2-x}Cu_x$ (x = 0, 0.1, 0.15 and 0.2) vs. Cu content and, (b) $GdFe_{2-x}Cr_x$ (x = 0, 0.1, 0.15 and 0.2) vs. Cr content.

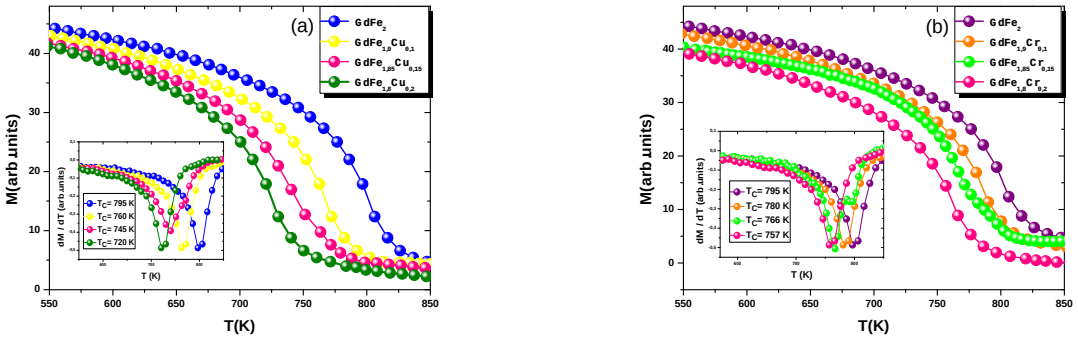

Figure 5. M(T) curves for (a) $GdFe_{2-x}Cu_x$ (x = 0, 0.1, 0.15 and 0.2) and, (b) $GdFe_{2-x}Cr_x$ (x = 0, 0.1, 0.15 and 0.2). Tne inset : dM/dT vs temperature.

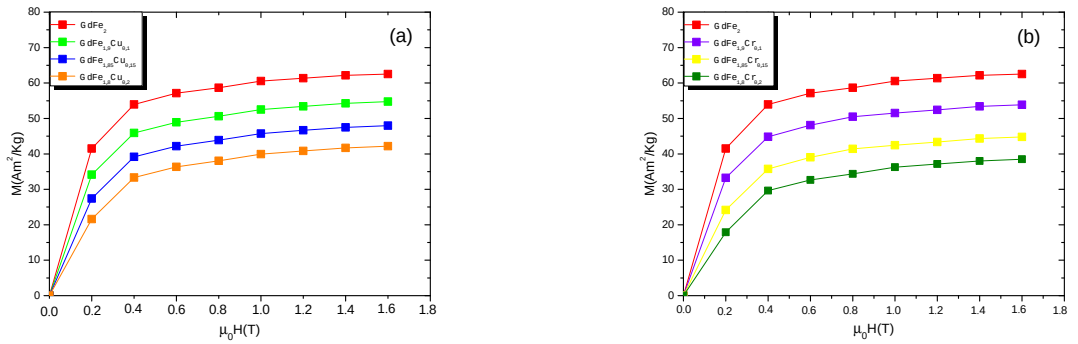

Figure 6. M(H) curves at T = 300 K for (a) $GdFe_{2-x}Cu_x$ (x = 0, 0.1, 0.15 and 0.2) and, (b) $GdFe_{2-x}Cr_x$ (x = 0, 0.1, 0.15 and 0.2) compounds.

leads to a slight increase of the lattice parameters. In addition, B. Kotur *et al.* [64] indicated that the substitution of iron by larger atoms (Titanium, Vanadium, Molybdenum) resulted in great enhancement of the lattice parameters as well as the hydrogen capacity of the $ErFe_{2-x}M_x$ compounds.

3.2 Magnetic properties

The magnetic transition temperatures of the $GdFe_{2-x}(Cu,Cr)_x$ (x = 0, 0.1, 0.15 and 0.2) compounds were identified by the temperature dependence of magnetization measurements $M(T)$ carried out in a low applied magnetic field of 0.12 T. All the studied samples present a sharp ferromagnetic-paramagnetic transition at Curie temperature. The plotted magnetization curves are illustrated in Figure 5. The values of the transition temperature T_C is defined from the minimum of the temperature derivative of the magnetization, dM/dT versus temperature.

Consequently, the substitution of Cu and Cr in the $GdFe_{2-x}(Cu,Cr)_x$ (x = 0, 0.1, 0.15 and 0.2) compounds has a striking effect on their magnetic ordering transition temperatures. From Figure 5, we can clearly see that T_C drops with the increasing Cu and Cr content. We believe that this decrease is caused by the magnetic dilution that results from the replacement of magnetic iron atoms by non-magnetic copper and chromium atoms. Likewise, W. Steiner *et al.* [65] have studied the effect of Al substitution by Fe on magnetic and structural properties of $Gd(Fe_{1-x}Al_x)_2$ compounds. They showed that T_C values decrease with increasing Al content from 795 K for $GdFe_2$ to 540 K for $Gd(Fe_{0.8}Al_{0.2})_2$. Similarly, a previous study by N.H. Duc *et al.* [66] of the $Gd(Fe,Ti)_2$ compounds reveals that the increase of Ti concentration causes a gradual reduction in Curie temperature until 750 K for x = 0.1.

The $M(H)$ curves at 300 K as a function of the applied magnetic field for different x values of $GdFe_{2-x}Cu_x$ and $GdFe_{2-x}Cr_x$ are shown respectively in Figure 6. From these curves, we have found that all the samples are magnetically ordered at 300 K and their magnetization depends on the copper and chromium concentration. Furthermore, the saturation magnetization M_S was obtained by fitting the isothermal magnetization against magnetic field plots using the saturation approach law [67] :

$$M = M_S\left(1 - \frac{b}{H^2}\right)$$

We notice that, M_S decreases with the substitution of iron by Copper atoms as follows: 62.16 Am^2/kg (2.99 μ_B) for x = 0; 54.26 Am^2/kg (2.62 μ_B) for x = 0.1; 47.50 Am^2/kg (2.29 μ_B) for x = 0.15 and 41.69 Am^2/kg (2.01 μ_B) for x = 0.2. Likewise, the substitution of iron by chromium atoms has the effect of reducing M_S as follows: 53.40 Am^2/kg (2.56 μ_B) for x = 0.1, 44.33 Am^2/kg (2.13 μ_B) for x = 0.15, and 37.99 Am^2/kg (1.82 μ_B) for x = 0.2. Curie temperature and saturation magnetization values of the $GdFe_{2-x}(Cu,Cr)_x$ (x = 0, 0.1, 0.15 and 0.2) compounds are displayed in Table 3.

Table 3. Values of Curie temperature and saturation magnetization for $GdFe_{2-x}(Cu, Cr)_x$ (x= 0, 0.1, 0.15 and 0.2) compounds.

Compounds	T_C (K)	M_S (Am^2/kg)
$GdFe_2$	795	62.16
$GdFe_{1.9}Cu_{0.1}$	760	54.26
$GdFe_{1.85}Cu_{0.15}$	745	47.50
$GdFe_{1.8}Cu_{0.2}$	720	41.69
$GdFe_{1.9}Cr_{0.1}$	780	53.40
$GdFe_{1.85}Cr_{0.15}$	766	44.33
$GdFe_{1.8}Cr_{0.2}$	757	37.99

3.3 Magnetocaloric properties

The magnetic refrigeration (MR) based on the magnetocaloric effect (MCE) is of potential impact in both the field of science and technology due to their energy saving nature and environmental friendliness [7, 8, 9, 10]. The MCE is an intrinsic property of magnetic materials and manifests itself in the heating or cooling of a magnetic material when undergoing a magnetic field. In this work, the magnetization isotherms $M(H)$ for $GdFe_{2-x}(Cu,Cr)_x$ (x = 0, 0.1, 0.15 and 0.2) single crystal compounds were measured in a wide range of temperatures around magnetic transition temperature T_C. Figure 7 presents the magnetization isotherms $M(H)$ of the $GdFe_2$, $GdFe_{1.8}Cu_{0.2}$ and $GdFe_{1.8}Cr_{0.2}$ compounds as an example. It could be noted that magnetization increases slowly with the applied field above the Curie temperature resulting in the paramagnetic behavior of the compounds. However, below the Curie temperature, the magnetization rises rapidly with the applied magnetic field resulting in the ferromagnetic state of the compounds.

The nature of magnetic phase transition of the $GdFe_{2-x}(Cu,Cr)_x$ (x = 0, 0.1, 0.15 and 0.2) compounds was identified by means of the Arrott-plots ($\mu_0 H/M$ vs. M^2) deduced from the magnetic field dependence of the isothermal magnetization. Arrott-plots of $GdFe_2$, $GdFe_{1.8}Cu_{0.2}$ and $GdFe_{1.8}Cr_{0.2}$ compounds are illustrated in Figure 8 as an example. In this Figure, there is neither S-shape curves nor negative slopes, which is indicative of a first order transition. However, in our experiment, we noted that these plots exhibit a positive slope demonstrating second-ordered phase characteristic of the ferromagnetic to paramagnetic transition as demonstrated by the Banerjee criterion [68].

To clarify the nature of the paramagnetic-ferromagnetic phase transition we used the Landau theory [69] and the Inoue-Shimizu model [70]. The magnetic free energy F can be expanded in power of magnetization M:

$$F(M,T) = \frac{1}{2}a(T)M^2 + \frac{1}{4}b(T)M^4 + \frac{1}{6}c(T)M^6 + \ldots - \mu_0 HM$$

where $a(T), b(T)$, and $c(T)$ are the Landau coefficients. The minimization of $F(M,T)$ with respect to M gives:

$$\mu_0 H = a(T)M + b(T)M^3 + c(T)M^5$$

The coefficient $a(T)$ presents a minimum at $T = T_C$, while the coefficient $b(T)$ can be positive, zero, or negative. When $b(T_C)$ is positive or null the magnetic phase transition is of the second order, whereas, a first order magnetic phase transition occurs when $b(T_C)$ is negative.

Figure 9 shows the evolution of the Landau coefficients $a(T)$ and $b(T)$ with the temperature for $GdFe_{1.8}Cu_{0.2}$ compound. We clearly observed that $b(T = T_C) = 0$, which means that $F(M,T)$ is minimum that corresponds to $M = 0$ and consequently confirms the second order phase transition.

Magnetic compounds that show SOMT exhibit very low thermal and magnetic hysteresis. They could therefore be candidates for magnetic cooling.

The MCE of the samples is characterized by the isothermal magnetic entropy change $\Delta S(T)$ as a function of temperature T and the applied magnetic field H. Indeed, the magnetic

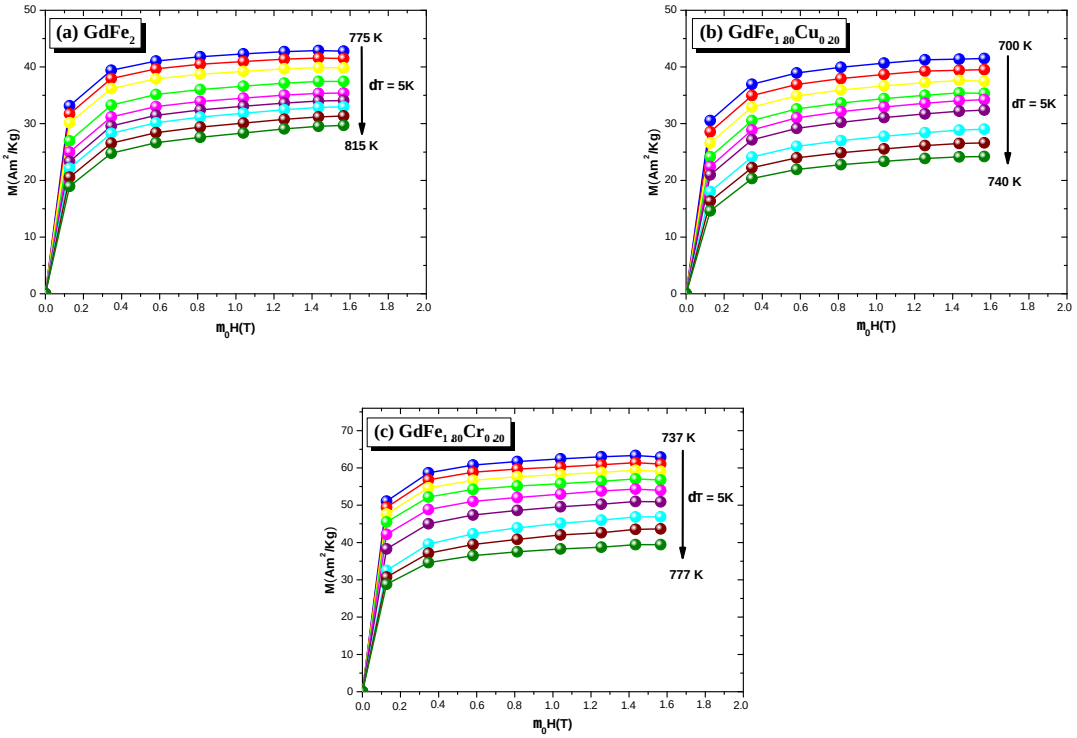

Figure 7. Isotherm magnetization curves $M(H, T)$ of (a) $GdFe_2$, (b) $GdFe_{1.8}Cu_{0.2}$ and (c) $GdFe_{1.8}Cr_{0.2}$ compounds.

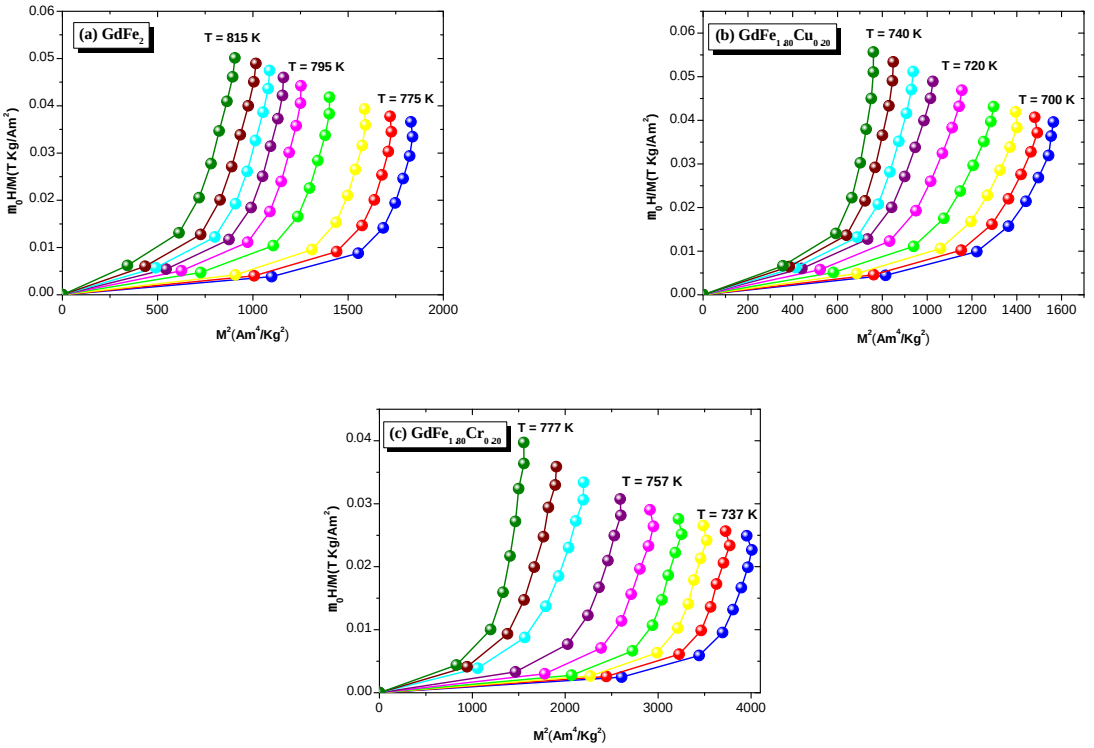

Figure 8. The Arrott plots of (a) $GdFe_2$, (b) $GdFe_{1.8}Cu_{0.2}$ and (c) $GdFe_{1.8}Cr_{0.2}$ compounds.

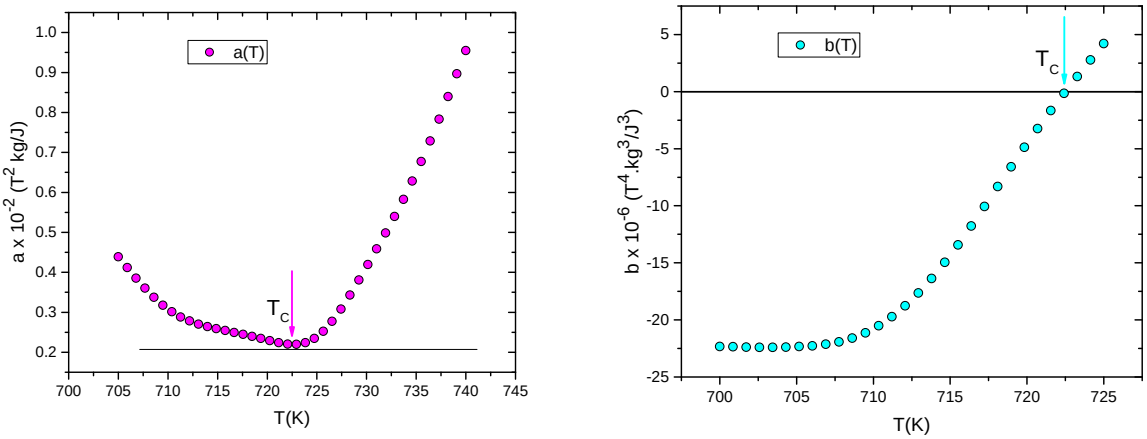

Figure 9. Temperature dependence of Landau coefficient $a(T)$ and $b(T)$ for $GdFe_{1.8}Cu_{0.2}$ compound.

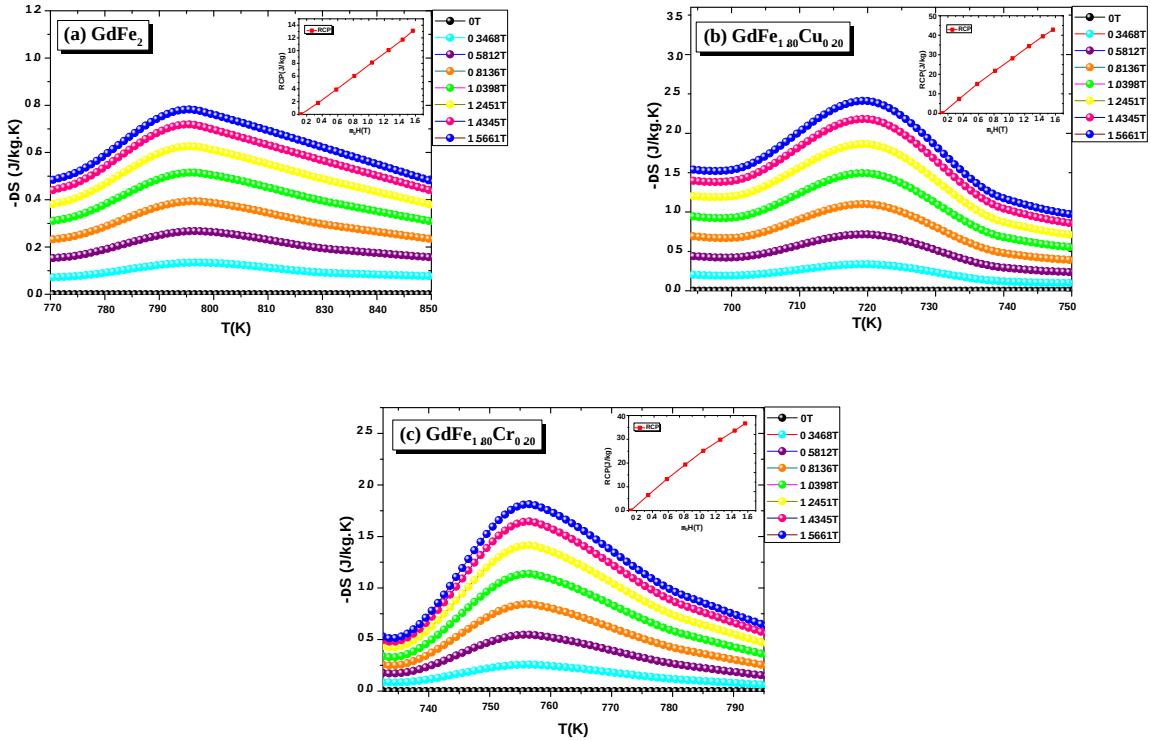

Figure 10. Entropy change of (a) $GdFe_2$, (b) $GdFe_{1.8}Cu_{0.2}$ and (c) $GdFe_{1.8}Cr_{0.2}$ compounds.

entropy change, $\Delta S(T)$ was calculated through the numerical integration of the isothermal magnetization curves $M(H,T)$ between $\mu_0 H = 0$ and $\mu_0 H = 1.56$ T, employing the following Maxwell's thermodynamic formula [71]:

$$\Delta S = \mu_0 \int_0^H (\frac{\partial M}{\partial T}) dH$$

$$\Delta S(T_i, \Delta H) = \mu_0 \sum_j \frac{M_{i+1}(T_{i+1}, H_j) - M_i(T_i, H_j)}{T_{i+1} - T_i} \Delta H_j$$

The magnetic entropy change plots measured at different temperatures under external field change for $GdFe_2$, $GdFe_{1.8}Cu_{0.2}$ and $GdFe_{1.8}Cr_{0.2}$ compounds are illustrated in Figure 10. It is clearly seen that the maximum magnetic entropy change at the magnetic ordering temperature for the $GdFe_2$ reaching a value of $\Delta S_{max} = 0.79$ J/kg K at $T_C = 795$ K leads to a pronounced increase as both copper and chromium content x increases. Meanwhile, the ΔS_{max} for $GdFe_{2-x}Cu_x$ samples are slightly higher than those measured for alloys $GdFe_{2-x}Cr_x$. For example, ΔS_{max} value for the $GdFe_{1.8}Cu_{0.2}$ sample is equal to 2.5 J/kg K, while ΔS_{max} value achieved for the $GdFe_{1.8}Cr_{0.2}$ sample is about 1.8 J/kg K.

The relative cooling power (RCP) is another crucial parameter that needs to be measured so as to determine the efficiency

Table 4. Values of maximum entropy variation $-\Delta S_{\max}$, relative cooling power RCP, and Temperature Averaged Entropy Change (TEC) for ΔT_{H-C} of 3 and 10 K, for $GdFe_{2-x}(Cu, Cr)_x$ (x= 0, 0.1, 0.15 and 0.2) compounds compared with other $R(Fe,Co)_2$ magnetic materials.

Compounds	$\mu_0 H$(T)	$-\Delta S_{\max}$ (J/kg.K)	RCP (J/kg)	TEC(3) (J/kg.K)	TEC(10)	reference
$GdFe_2$	1.5	0.79	13.3	1.46	1.15	This work
$GdFe_{1.9}Cu_{0.1}$	1.5	1.2	21.6			This work
$GdFe_{1.85}Cu_{0.15}$	1.5	1.4	31.7			This work
$GdFe_{1.8}Cu_{0.2}$	1.5	2.5	44.3	2.17	1.53	This work
$GdFe_{1.9}Cr_{0.1}$	1.5	0.9	14.8			This work
$GdFe_{1.85}Cr_{0.15}$	1.5	1.3	25.4			This work
$GdFe_{1.8}Cr_{0.2}$	1.5	1.8	36.8	2.85	2.12	This work
$HoFe_{0.4}Co_{1.6}$	1.5	0.5	–	–	–	[75]
$HoFe_{0.14}Co_{1.86}$	1.5	1.5	–	–	–	[75]
$ErFe_{0.1}Co_{1.9}$	1	3	–	–	–	[73]
$ErFe_{0.2}Co_{1.8}$	1	1	–	–	–	[73]
$TbFe_{0.1}Co_{1.9}$	5	3.5	–	–	–	[74]
$DyFe_{0.08}Co_{1.92}$	2	2.5	–	–	–	[76]

and the suitability of corresponding magnetocaloric materials for magnetic cooling. This factor is defined as the transferring of heat from the cold sink to the hot one in a refrigerant cycle. RCP is determined as a product of the full-width half maximum value in $\Delta S_{\max}$) curves and the maximum peak value of the entropy change, and is given by the below equation [72]:

$$RCP = -\Delta S_{\text{Max}} \times \delta T_{FWHM}$$

The field change dependence of the RCP for $GdFe_2$, $GdFe_{1.8}Cu$ and $GdFe_{1.8}Cr_{0.2}$ compounds is summarized in the inset of Figure 10. The calculated $-\Delta S_{\max}$, and RCP parameters extracted from magnetocaloric study of all the studied compounds are listed in Table 4. From on this table, we can see that the RCP of $GdFe_{2-x}Cu_x$ (x= 0, 0.1, 0.15 and 0.2) compounds rise up monotonically as the copper concentration increases from 13.3 J/kg K to 44.3 J/kg K for x = 0 and x = 0.2, respectively. Similarly, the chromium substitution increases in effective way the RCP value of $GdFe_{2-x}Cr_x$ (x= 0, 0.1, 0.15 and 0.2) alloys. Because of the high value of Curie temperature, the $GdFe_{2-x}(Cu,Cr)_x$ alloys are qualified to be a significant candidate for magnetic refrigeration applications at high temperature (heat pump). The values of the magnetic entropy of the $GdFe_{2-x}(Cu,Cr)_x$ system are close to those determined in the $R(Fe,Co)_2$ system [73, 74, 75, 76].

In order to improve the definition of the figure of merit and to make it more relevant, a new Temperature Averaged Entropy Change (TEC) parameter was proposed [77, 78, 79, 80, 81]. TEC can be derived using the following relation:

$$\text{TEC}(\Delta T_{H-C}) = \frac{1}{\Delta T_{H-C}} \max \left\{ \int_{T_{mid}-\frac{\Delta T_{H-C}}{2}}^{T_{mid}+\frac{\Delta T_{H-C}}{2}} |\Delta S_M(T)| dT \right\}$$

where $\Delta T_{H-C} = T_{Hot} - T_{Cold}$, T_{mid} was chosen to optimize $\text{TEC}(\Delta T_{H-C})$. The calculated TEC values are given in Table 4.

We can notice, on the one hand, that the Temperature Averaged Entropy Change decreases with increasing ΔT_{H-C}, and on the other hand, the substitution of Fe by Cr or Cu atoms increases the TEC value, in another words, the magnetocaloric efficiency is increased. In addition, the RCP parameter generally overestimate the magnetocaloric effect merit of intermetallics with a second-order phase transition.

4. Conclusion

The present paper explores the series of compounds $GdFe_{2-x}(Cu, Cr)_x$ (x= 0, 0.1, 0.15 and 0.2) with the aim of investigating their structural, magnetic and magnetocaloric properties. Room temperature X-ray powder diffraction analysis demonstrates that the crystal structure of all the synthesized compounds belongs to the cubic Laves-phase with $MgCu_2$-type structure ($Fd\bar{3}m$ space group). Indeed, the crystal structure of the parent compound $GdFe_2$ was found to stay conserved for all the melting alloys. The effect of substituting iron atoms in $GdFe_2$ with larger copper atom, leads to a rise in the lattice parameter a and the unit cell volume V. In contrast, these parameters decrease linearly with the increasing chromium atom. The study of the magnetic properties of the $GdFe_{2-x}(Cu, Cr)_x$ (x= 0, 0.1, 0.15 and 0.2) compounds revealed that the Curie temperature reduces with Cu and Cr substitutions. In fact, this decrease is due to the substitution of magnetic atoms by non-magnetic ones. The positive slopes of the Arrott plots for the substituted compounds indicate that the phase transition from ferromagnetic to paramagnetic state around T_C undergo a second-order phase transition. Emphasis is mainly given to the study of magnetocaloric performances in the vicinity of magnetic phase transition in terms of the maximum magnetic entropy change and the relative cooling power. It is significant to note that a pronounced enhancement of the values of $-\Delta S_{\max}$ and RCP of such substituted compounds occurs with the increase of copper and chromium content. A

Mössbauer spectrometry study will be performed to confirm the structural properties and to determine the local magnetic moment per inequivalent crystallographic site. Moreover, ab-initio calculations of the electronic structure will be carried out to determine the theoretical magnetic moments and hyperfine fields in order to compare them with those derived by Mössbauer spectrometry.

5. Acknowledgments

This work was mainly supported by the CNRS, ICMPE, France, and the Tunisian Ministry of Higher Education and Scientific Research and Technology, LSME, University of Sfax, Tunisia.

References

[1] X. Chen, S Omer, M. Worall, and S. Riffat. *J. Renew. Sust. Energ. Rev.*, 19:629, 2013.

[2] J. R. Gómez, R. F. Garcia, J. C. Carril, and M. R. Gómez. *Int. J. Refrigeration.*, 36:1388, 2013.

[3] E. Brück, O. Tegus, D. T. C. Thanh, and K. H. J .Buschow. *J. Magn. Magn. Mater.*, 310:2793, 2007.

[4] E. Brück. *J. Phys. D: Appl. Phys.*, 38:R381, 2005.

[5] M. A. Benedict, S. A. Sherif, M. Schroeder, and D. G. Beers. *Int. J. Refrigeration.*, page 20, 2017.

[6] J. R. Gómez, R. F. Garcia, A. D. M. Catoira, and M. R. Gómez. *J. Renew. Sust. Energ. Rev.*, 17:74, 2012.

[7] P. V. Trevizoli and Jr J. R. Barbosa. *Reference Module in Materials Science and Materials Engineering.*, 2020.

[8] Q. H. Shi, C. L. Xue, C. J. Fan, L. L. Yan, N. Qiao, M. Fang, and S. F. Wang. *Polyhedron.*, 194:114938, 2021.

[9] M. Arejdal. *Results Phys.*, 18:114938, 2020.

[10] L. Li and M. Yan. *J. Alloys Compd.*, 823:153810, 2020.

[11] V. Franco, J. S. Blazqueza, J. J. Ipus, J. Y. Law, L. M. Moreno-Ramirez, and A. Conde. *J. Prog. Mater. Sci.*, 93:112, 2018.

[12] K. A. Gschneidner, V. K. Pecharsky, and A. O. Tsokol. *Rep. Prog. Phys.* , 68:1479, 2005.

[13] A. Bartok, M. Kustov, L. F. Cohen, A. Pasko, K. Zehani, L. Bessais, F. Mazaleyrat, and M. Lobue. *J. Magn. Magn. Mater.*, 400:333, 2016.

[14] R. Guetari, R. Bez, C. B. Cizmas, N. Mliki, and L. Bessais. *J. Alloys Compd.*, 579:156, 2013.

[15] S. Walha, M. Jemmali, R. Skini, H. Noél, E. Dhahri, R. Hassen, and E. K. Hlil. *J. Supercond. Nov. Magn.*, 27:2131, 2014.

[16] R. Guetari, R. Bez, A. Belhadj, K. Zehani, A. Bezergheanu, N. Mliki, L. Bessais, and C. B. Cizmas. *J. Alloys Compd.*, 588:64, 2014.

[17] S. Gupta, K.G. Suresh, and A.V. Lukoyanov. *J. Mater Sci.*, 50:5723, 2015.

[18] S. Charfeddine, K. Zehani, L. Bessais, and A. Korchef. *J. Solid State Chem.*, 238:15, 2016.

[19] K. Nouri, M. Jemmali, S. Walha, K. Zehani, A. Ben Salah, and L. Bessais. *J. Alloys Compd.*, 672:440, 2016.

[20] W. Bouzidi, N. Mliki, and L. Bessais. *J. Magn. Magn. Mater.*, 441:566, 2017.

[21] N. Bouchaala, M. Jemmali, T. Bartoli, K. Nouri, I. Hentech, S. Walha, L. Bessais, and A. Ben Salah. *J. Solid State Chem.*, 258:501, 2018.

[22] S. Pakhira, C. Mazumdar, D. Choudhury, R. Ranganathan, and S. Giri. *Phys. Chem. Chem. Phys.*, 20:13580, 2018.

[23] M. Saidi, K. Nouri, S. Walha, E. Dhahri, A. Kabadou, M. Jemmali, and L. Bessais. *J. Electron. Mater.*, 48:2242, 2019.

[24] M. Saidi, S. Walha, E. K. Hlil, L. Bessais, and M. Jemmali. *J. Solid State Chem.*, 297:122019, 2021.

[25] V. K. Pecharsky and K. A. Gschneidner. *Phys. Rev. Lett.*, 78:4494, 1997.

[26] J. H. Belo, A. M. Pereira, J. Ventura, G. N. P. Oliveira, J. P. Araújo, P. B. Tavares, L. Fernandes, P. A. Algarabel, C. Magen, L. Morellon, and M. R. Ibarra. *J. Alloys Compd.*, 529:89, 2012.

[27] X. B. Liu and Z. Altounian. *J. Appl. Phys.*, 99:08Q101, 2006.

[28] Y. Long, Z. Y. Zhang, D. Wen, G. H. Wu, R. C. Ye, Y. Q. Chang, and F. R. Wan. *J. Appl. Phys.*, 98:033515, 2005.

[29] H. R. Khan and O. Loebich. *Physica C.*, 153:433, 1988.

[30] K. Nouri, M. Saidi, S. Walha, L. Bessais, and M. Jemmali. *Chem. Afr.*, 3:111, 2020.

[31] C. D. Rabadia, Y. J. Liu, L. Y. Chen, S. F. Jawed, L. Q. Wang, H. Sun, and L. C. Zhang. *Mater. Des.*, 179:107891, 2019.

[32] S. S. Mishra, T. P. Yadav, O. N. Srivastava, N. K. Mukhopadhyay, and K. Biswas. *J. Alloys Compd.*, 832:153764, 2020.

[33] C. Jiang. *Acta Mater.*, 55:1599, 2007.

[34] J. D. Livingston and E. L. Hall. *J. Mater. Res.*, 5:5, 1990.

[35] D. Fruchart, A. Rouault, C. B. Shoemaker, and D. P. Shoemaker. *J. Less-Common. Met.*, 73:363, 1980.

[36] C. W. Zhang. *Physica B.*, 403:2088, 2008.

[37] J. Radakovic, J. Belosevic-Cavor, and V. Koteski. *Int. J. Hydrog. Energy.*, 38:9229, 2013.

[38] C. L. Wang, J. Liu, Y. Mudryk, K. A. Gschneidner Jr, Y. Long, and V. K. Pecharsky. *J. Magn. Magn. Mater.*, 405:122, 2016.

[39] N. Duc, D. K. Anh, and P. Brommer. *Physica B Condens. Matter.*, 319:1, 2002.

[40] Y. Zhuang, J. Deng, J. Li, Y. Zhan, Q. Zhu, and K. Zhou. *Rare Metals.*, 26:97, 2007.

[41] M. Halder, S. M. Yusuf, M. D. Mukadam, and K. Shashikala. *Phys. Rev. B.*, 81:174402, 2010.

[42] K. W. Zhou, Y. H. Zhuang, J. Q. Li, J. Q. Deng, and Q. M. Zhu. *Solid State Commun.*, 137:275, 2006.

[43] I. A. Al-Omari, M. A. Al-Akhras, M. K. Hasan, J. Shobaki, and K. A. Azez. *J. Alloys Compd.*, 319:34, 2001.

[44] I.A. Al-Omari and S. Aich. *J. Alloys Compd.*, 375:31, 2004.

[45] G. M. Elalfy, R. M. Shabara, S. H. Aly, and S. Yehia. *Comput. Condens. Matter.*, 5:24, 2015.

[46] M. Saidi, S. Walha, K. Nouri, A. Kabadou, M. Jemmali, and L. Bessais. *J. Alloys Compd.*, 781:159, 2019.

[47] M. Saidi, S. Walha, K. Nouri, A. Kabadou, L. Bessais, and M. Jemmali. *J. Alloys Compd.*, 792:87, 2019.

[48] H. Rietveld. *Acta Crystallogr.*, 22:151, 1967.

[49] H. Rietveld. *J. Appl. Crystallogr.*, 2:65, 1969.

[50] J. Rodriguez-Carvajal. *Physica B* , 192:55, 1993.

[51] J. Rodriguez-Carvajal, M. T. Fernandez-Diaz, and J. L. Martinez. *J. Phys.* , 81:210, 2000.

[52] L. Bessais, S. Sab, C. Djega-Mariadassou, N. H. Dan, and N. X. Phuc. *Phys. Rev. B*, 70:134401, 2004.

[53] S. Khazzan, N. Mliki, L. Bessais, and C. Djega-Mariadassou. *J. Magn. Magn. Mater.*, 322:224, 2010.

[54] K. Zehani, A. Bez, A. Boutahar, EK Hlil, H. Lassri, J. Moscovici, N. Mliki, and L. Bessais. *J. Alloys Compd.*, 591:58–64, 2014.

[55] N. Hosni, K. Zehani, T. Bartoli, and L. Bessais H. Maghraoui-Meherzi. *J. Alloys Compd.*, 694:1295–1301, 2017.

[56] M. Phejar, V. Paul-Boncour, and L. Bessais. *J. Solid State Chem.*, 223:95–102, 2016.

[57] P. Villars and L.D. Calvert. *Pearsons handbook of crystallographic data for intermetallic phases, 2nd ed. Materials Park, OH: ASM*, 1991.

[58] D. J. Thoma, F. Chu, P. Peralta, P. G. Kotula, K. C. Chen, and T. E. Mitchell. *Mater. Sci. Eng. A.*, 239:251, 1997.

[59] B. M. Klein, W. E. Pickett, D. A. Papaconstantopoulos, and L. L. Boyer. *Phys. Rev. B.*, 27:6721, 1983.

[60] J. Cwik, Y. Koshkidko, N. A. de Oliveira, K. Nenkove, A. Hackemer, E. Dilmieva, N. Kolchugina, S. Nikitin, and K. Rogacki. *Acta Mater.*, 133:230, 2017.

[61] J. B. Friauf. *Phys Rev.*, 29:34, 1927.

[62] K. H. J. Buschow. *Rep. Prog. Phy.*, 40:1179, 1977.

[63] Z. Li, H. Wang, L. Ouyang, J. Liu, and M. Zhu. *J. Alloys Compd.*, 689:843, 2016.

[64] B. Kotur, O. Myakush, and I. Zavaliy. *J. Alloys Compd.*, 442:17, 2007.

[65] W. Steiner. *J. Magn. Magn. Mater.*, 14:47, 1979.

[66] N. H. Duc, M. M. Tan, N. D. Tan, D. Givord, and J. Teillet. *J. Magn. Magn. Mater.*, 177:1107, 1998.

[67] L. Néel. *J. Phys. Radium*, 9:148, 1948.

[68] S. K. Banerjee. *Phys.Lett.*, 16:12, 1964.

[69] A. Arrott and J. Noakes. *Phys. Rev. Lett.*, 19:786, 1967.

[70] J. Inoue and M. Shimizu. *J. Phys. F*, 12:1811, 1982.

[71] M. Foldeaki, R. Chahine, and T. K. Bose. *J. Appl. Phys.*, 77:3528, 1995.

[72] V. K. Pecharsky and K. A. Gschneidner. *J. Appl. Phys.*, 86:565, 1999.

[73] X. B. Liu and Z. Altounian. *J. Appl. Phys.*, 103:07B304, 2008.

[74] Madhumita Halder, S. M. Yusuf, M. D. Mukadam, and K. Shashikala. *Phys. Rev. B*, 81:174402, 2010.

[75] Maksim Anikin, Evgeniy Tarasov, Nikolay Kudrevatykh, Aleksander Inishev, Aleksander Zinin, Aleksander Teplykh, and Aleksander Pirogov. *Physics Procedia*, 75:1198–1206, 2015.

[76] Maksim Anikin, Evgeniy Tarasov, Nikolay Kudrevatykh, Aleksander Inishev, M. Semkin, A. Volegov, and Aleksander Zinin. *J. Magn. Magn. Mater.*, 418:181–187, 2016.

[77] L. D. Griffith, Y. Mudryk, J. Slaughter, and V. K. Pecharsky. *J. Appl. Phys.*, 123:034902, 2018.

[78] A. Sakka, R. M'nassri, Muaffaq M. Nofal, S. Mahjoub, W. Cheikhrouhou-Koubaa, N. Chniba-Boudjada, M. Oumezzine, and A. Cheikhrouhou. *J. Magn. Magn. Mater.*, 514:167158, 2020.

[79] S. Choura-Maatar, Muaffaq M. Nofal, R. M'nassri, W. Cheikhrouhou-Koubaa, N. Chniba-Boudjada, and A. Cheikhrouhou. *J. Mater. Sci.: Mater. Electron.*, 31:1634–1645, 2020.

[80] L. Su, X. Q. Zhang, Q. Y. Dong, H. T. Yang, S. H. Li, and Z. H. Cheng. *Ceram. Int.*, 47:18286–18294, 2021.

[81] D. Mazumdar and I. Das. *J. Appl. Phys.*, 129:063901, 2021.